Organic Electronics 132 (2024) 107095

Contents lists available at ScienceDirect

Organic Electronics

journal homepage: www.elsevier.com/locate/orgel

Computational screening of multi-resonance thermally activated delayed fluorescence (MR-TADF) molecules for lasing application

Rongrong Li [a], Zhigang Shuai [a,b,*]

[a] School of Science and Engineering, The Chinese University of Hong Kong, Shenzhen, Guangdong 518172, PR China
[b] MOE Key Laboratory of Organic OptoElectronics and Molecular Engineering, Department of Chemistry, Tsinghua University, Beijing 100084, PR China

ARTICLE INFO

Keywords:
Multi-resonance thermally activated delayed fluorescence
Laser candidate molecules
Theoretical descriptor
Density functional theory
Time-dependent density functional theory

ABSTRACT

Multi-resonance thermally activated delayed fluorescence (MR-TADF) molecules charactering large emission oscillator strengths, effective reverse intersystem crossing (RISC), and narrow emission spectral width, have great potential as laser materials. We propose a molecular descriptor for quick screening MR-TADF molecules as laser candidate materials, $A = \Delta E_{ST}\sigma_{eff}^{net,opt}$, namely, the product of singlet-triplet energy gap and the optical pumping net stimulated emission cross section. These quantities can be calculated by combining quantum chemistry package Gaussian and our own MOMAP program. Through extensive computations benchmarked with existing experiments, we suggest that A value should be larger than 0.311×10^{-17} cm^2 eV for promising lasing molecules. We virtually designed 119 molecules with MR-TADF property, and based on our theoretical protocol by considering descriptor A, we are able to select 10 molecules as lasing molecules. We then further screen out 2 molecules through analyzing the spectral overlap, indicating that only eight molecules are prospective candidates for laser materials. Particularly, we find that ADBNA-Me-BPy molecule possesses large radiative decay rate and large reverse intersystem crossing rate, 1.90×10^6 s^{-1} and 1.01×10^8 s^{-1}, respectively, implying a low lasing threshold, promising for electrically pumped lasing.

1. Introduction

Since the first dye-doped organic solid-state laser (OSSL) was reported in 1966, OSSLs have attracted widespread attention due to its low cost, high photoluminescence (PL) efficiency, high PL wavelength range from ultraviolet to infrared, and flexible molecular structures design [1–5]. A large number of organic materials based on different organic small molecules or polymers were developed and applied to lasers [6,7]. Compared with optically pumped organic lasers, electric-driven OSSLs still have great challenges [8]. Recombination of injected electrons and holes would generate 25 % singlet and 75 % triplet excitons based on spin statistics in the electroluminescence process [9]. The long-lived triplet excitons are prone to accumulate and undergo triplet−triplet absorption (TTA), which leads to light amplification quenching [10]. And singlet−triplet annihilation will reduce singlet excitons [5]. Other species not involved in optical pumping lasers, such as polarons and excitons, also can cause multiple annihilation and absorption [5,11]. It is significant to develop organic gain materials that can improve the utilization efficiency of triplet excitons.

Both thermally activated delayed fluorescent (TADF) and phosphorescent materials can effectively utilize triplet excitons, resulting in nearly 100 % internal quantum efficiency under current injection [12–15]. Most phosphorescent materials are limited to inorganic compounds or expensive organometallic complexes, which dramatically increases application limitations and economic costs [11–13]. TADF emitters with a small singlet-triplet energy gap, could capture both S_1 and T_1 excitons through an efficient reverse intersystem crossing (RISC) process [14,15]. However, the charge transfer (CT) characters from S_1 to S_0 greatly suppresses the oscillator strength of TADF molecules [16–18], which directly leads to a small emission cross section and effects light amplification. Hatakeyama and co-workers proposed a “multi-resonance thermally activated delayed fluorescence (MR-TADF)” molecule with spatially separated frontier molecular orbitals, overcoming the disadvantage of small oscillator strength of TADF molecules [19].

In recent years, TADF and MR-TADF have been widely studied as the most promising emitters in photoluminescent materials and electroluminescent devices, while the reports as laser gain media are very limited [20–22]. This is because that current TADF molecules as laser materials

* Corresponding author. School of Science and Engineering, The Chinese University of Hong Kong, Shenzhen, Guangdong 518172, PR China.
E-mail addresses: shuaizhigang@cuhk.edu.cn, zgshuai@tsinghua.edu.cn (Z. Shuai).

https://doi.org/10.1016/j.orgel.2024.107095
Received 20 May 2024; Received in revised form 1 July 2024; Accepted 15 July 2024
Available online 16 July 2024
1566-1199/

require a higher light-pumping threshold than prompt fluorescence materials, much less the electrically pumped lasing [23,24]. The slow RISC rate and the small Stokes shift of MR-TADF molecules simply as optically pumped laser materials, caused serious self-absorption [25]. Molecular design descriptors for screening potential molecular structures and guiding the development of novel TADF and MR-TADF molecules as laser gain materials are urgent and significant.

In this paper, we report a theoretical descriptor for the molecular design and prediction of laser performance of MR-TADF molecules based on our group previously reported the computational screen-out protocol and TADF and MR-TADF candidate molecules for laser materials [26,27]. The proposed descriptor A, comprehensive considering the singlet-triplet energy gap (ΔE_{ST}), which could promote an effective RISC, and optical pumping net emission cross section ($\sigma_{eff}^{net,opt}$), can be used as a criterion to quickly screen out molecules with optically pumped laser properties. Density functional theory (DFT) and time-dependent DFT (TD-DFT) are performed to calculate the electronic structures and evaluate the absorption and emission wavelengths and corresponding oscillator strengths. With the criterion of descriptor, A and the photophysical parameters calculated by the thermal vibration correlation function (TVCF) formalism [28] in our home-built molecular material property prediction software package (MOMAP) [29,30], we evaluated the electronic structure and laser properties of 119 MR-TADF molecules (Fig. 1), and screened out 8 potential candidate molecules for laser materials.

2. Methodological approach

The Gaussian 16 suite of ab initio programs [31] was employed to perform DFT and TD-DFT calculation for B3LYP-D3, referring to the benchmark calculations in previous studies [27,32,33]. Unless otherwise noted, all computations in this work use the 6-31G(d) basis set [34]. The ground state geometry optimizations and vibrational frequency calculations are performed at B3LYP-D3/6-31G(d) level. The excited geometry optimizations of S_1 and T_1 are calculated by using TD-DFT and unrestricted open-shell DFT at the same level, respectively. The ΔE_{ST} value is obtained from B3LYP-D3/def2-TZVP of S_1 [32,33,35,36] and BMK/def2-TZVP of T_1 [35–37] for DABNA derivatives and TPSSh/def2-TZVP of S_1 [35,36,38] and PBE38/def2-TZVP of T_1 [35,36,39] for ADBNA derivatives. The spin−orbit coupling is evaluated at the same level at S_1 and T_1 optimized geometry, respectively, in the Q-Chem 5.3 program [40]. All rate constant calculations are performed via thermal vibration correlation function (TVCF) method in MOMAP 2020B [41], which has been successfully applied in a wide range to predict various optoelectrical properties of organic molecules.

3. Results and discussion

3.1. Theoretical descriptor and corresponding range of values

Based on the research through extensive computations benchmarked with existing experiments reported by our group [26,27], MR-TADF molecules, DABNA-2, ADBNA-Me-Mes, ADBNA-Me-Tip and ADBNA-Me-MesF (Fig. 2a), as the potential laser materials have the similar geometric configurations. And the products of $\sigma_{eff}^{net,opt}$ and ΔE_{ST} are stable at the constant 0.490. Fig. 2b shows the corresponding product distribution with a variance of only 9.2×10^{-5}. The small singlet-triplet energy gap will effectively promote the RISC process, which is beneficial for establishing population inversion to form four-energy level system. A larger optical pumping net emission cross section directly determines the light amplification. Both singlet-triplet energy gap, ΔE_{ST}, and optical pumping net emission cross section, $\sigma_{eff}^{net,opt}$, are significant parameters for MR-TADF laser molecules [27,48].

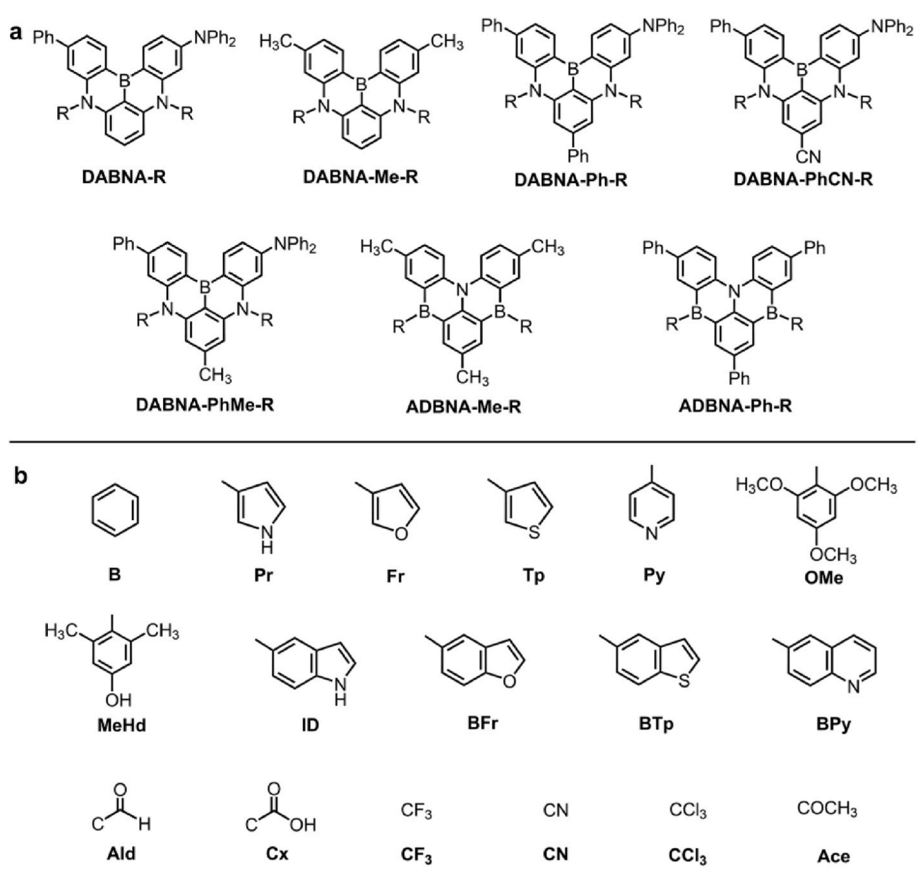

Fig. 1. The body (a) and substituent (b) of the designed MR-TADF molecular structures.

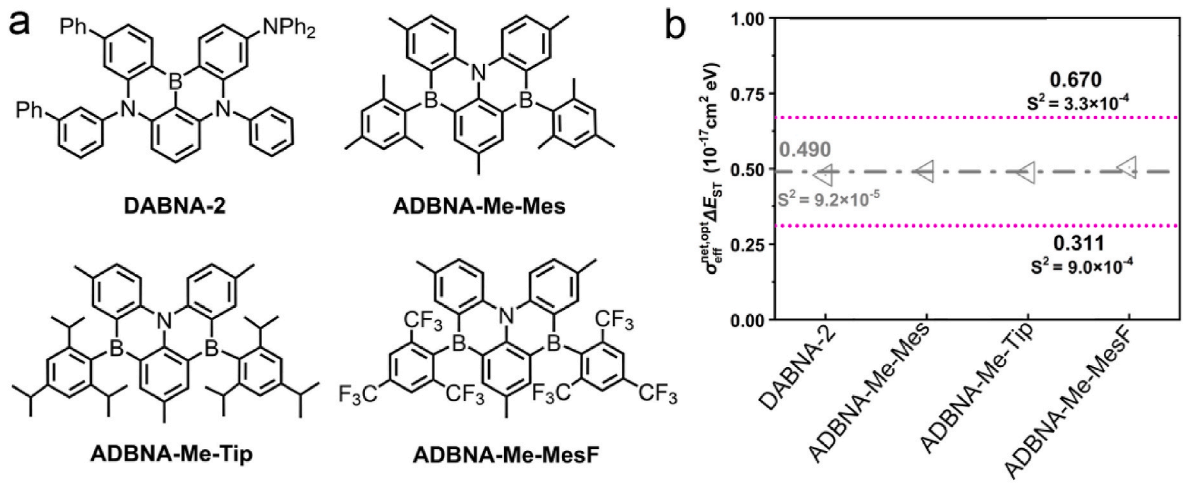

Fig. 2. Molecular structures (a) and the value of descriptor *A* (b) of MR-TADF molecules.

The characteristic that the product of ΔE_{ST} and $\sigma_{eff}^{net,opt}$ is constant can assist in determining whether this MR-TADF molecule can be used as a potential laser material. Therefore, the theoretical descriptor *A* is defined, where *A* is equal to the product of ΔE_{ST} and $\sigma_{eff}^{net,opt}$. Considering the error of the measurement of the emission cross section in the experiment, the value of the emission cross section is allowed to fluctuate within $\pm 1 \times 10^{-17}$ cm^2 and the fluctuated values are displayed in columns five and six in Table S1. The theoretical descriptor *A* has corresponding values ranging from 0.311×10^{-17} to 0.670×10^{-17} cm^2 eV, as shown by the pink dashed line in Fig. 2b. The MR-TADF molecule already has a relatively small ΔE_{ST}, and the space for ΔE_{ST} to decrease is small. That a large emission cross section is beneficial for light amplification is indisputable. Therefore, the value of descriptor *A* should be larger than 0.311×10^{-17} cm^2 eV for promising MR-TADF lasing molecules. The detailed ΔE_{ST}, optical pump net emission cross section $\sigma_{eff}^{net,opt}$, and the value of descriptor *A* of four molecules are shown

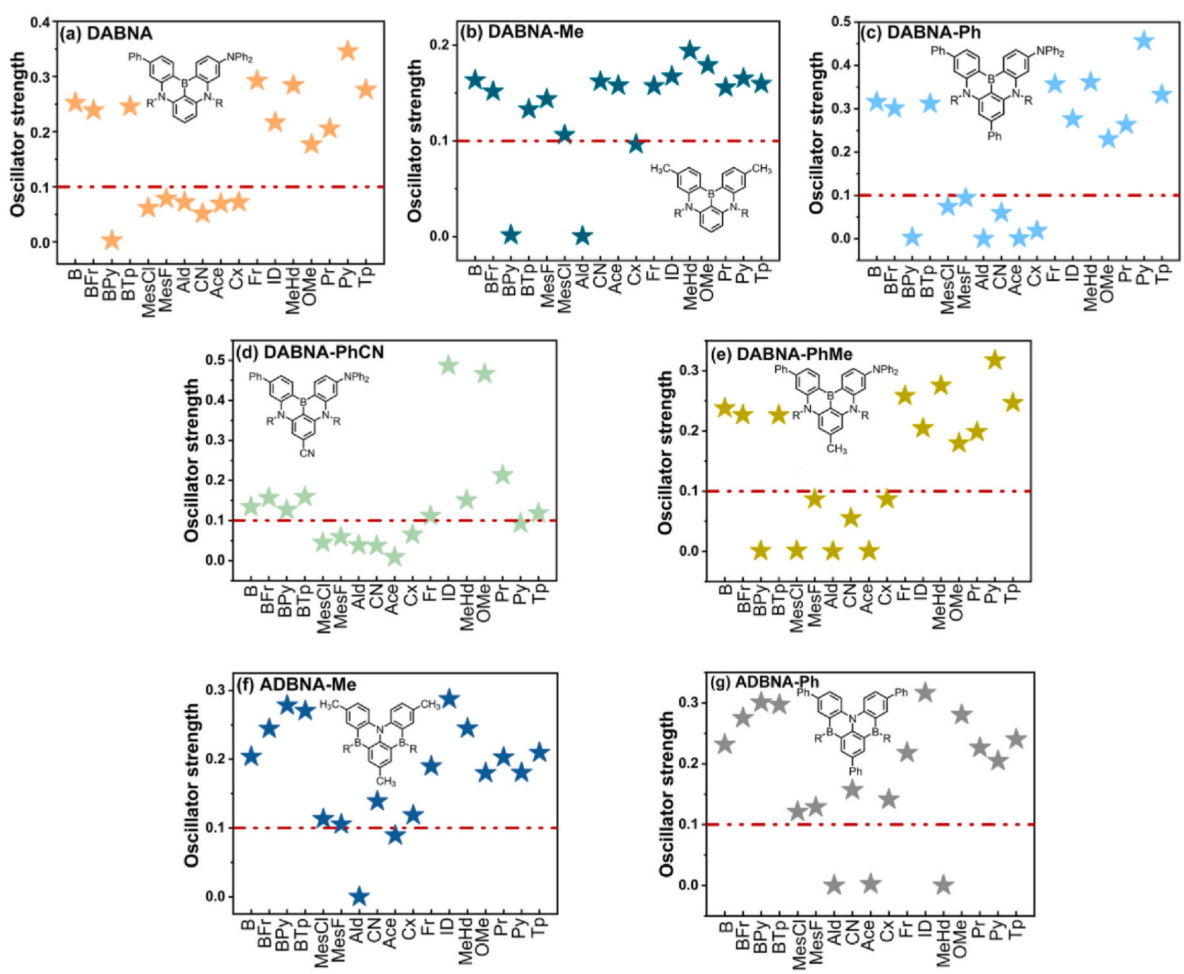

Fig. 3. The predicted emission oscillator strength of designed 119 MR-TADF molecules.

in Table S1 in supporting information.

3.2. Predicted emission oscillator strength

The investigated molecules are displayed in Fig. 1. Every body structure (Fig. 1a) could be linked to a substituent (Fig. 1b) and form 119 MR-TADF molecules. The emission oscillator strength is directly proportional to the emission cross section and descriptor A, so we first screen out molecules with very low f_{em} [48]. The calculated emission oscillator strengths of 119 molecules are plotted in Fig. 3. Some obviously unreasonable molecules with almost zero oscillator strength are excluded. Referring to the oscillator strength of experimentally reported MR-TADF molecules [27], molecules with f_{em} less than 0.1 are further excluded. As a result, 36 molecules were excluded as the candidates for organic laser materials due to their small oscillator strength.

3.3. The application of descriptor A

After preliminary screened by the emission oscillator strength, the value of descriptor A of the remaining molecules are calculated. The second-order approximate coupled cluster (SCS-CC2) method for ΔE_{ST} calculated is accurate [42]. However, applying this method to the large number of molecules we investigated is too expensive. The higher accuracy of ΔE_{ST} calculated by SCS-CC2 is due to the consistent error between the excitation energies of S_1 and T_1 [43]. And the different errors in calculated excitation energies between S_1 and T_1 result in poor accuracy of TD-DFT [43]. It should exist two different functions with the similar error for the excitation energy of S_1 and T_1. We attempted the TD-DFT method to calculate the emission energy of S_1 and T_1, respectively, with the aim of finding such two functions to predict the ΔE_{ST} with relative precision. Seven different density functions with different percentages of Hartree-Fock exchanges, including TPSSh [38], PBE38 [39], PBE0-1/3 [44], PW6B95 [45], PBE0 [46], BMK [37] and B3LYP [32] with Grimme's GD3 dispersion correction (-D3) [33], and the triple-zeta level def2-TZVP basis set [35,36], are performed to calculate the emission energy of DABNA-2 and corresponding three derivatives, and ADBNA-Me-R (R = Mes, Tip, MesF) [47], respectively. The emission energy of S_1 and T_1 obtained from B3LYP-D3 and BMK, respectively, for DABNA derivatived molecules, are reasonable. The mean absolute error (MAE) of ΔE_{ST} is only 0.038 eV compared with experimental values. For ADBNA derivatived molecules, the resulting MAE of ΔE_{ST} with S_1 and T_1 calculated by TPSSh and PBE38, respectively, is even smaller of 0.025 eV compared with experimental values. The emission energies, the values of ΔE_{ST}, molecular structures, and the average errors for different functions are shown in Table S2–S3, Table S4, Fig. S1 and Fig. S2 in supporting information, respectively.

Theoretically, laser emission cross section σ_{em} is proportionate to the emission oscillator strength f_{em} via [48]

$$\sigma_{em}(\upsilon) = \frac{e^2}{4\varepsilon_0 m_e c_0 n_F} g(\upsilon) f_{em} \tag{1}$$

Where e is the electron charge, ε_0 is the vacuum permittivity, m_e is the electron mass, c_0 is the speed of light, n_F is the refractive index of the gain material, υ is the corresponding emission frequency, and $g(\upsilon)$ is the normalized line shape function with $\int g(\upsilon)\,d\upsilon = 1$. The σ_{em} is rewritten as a function of wavelength by inserting $g(\upsilon) = \frac{g(\lambda)d\lambda}{d\upsilon} = g(\lambda)\frac{\lambda^2}{c_0}$ into eq (1):

$$\sigma_{em}(\lambda) = \frac{e^2\lambda^2}{4\varepsilon_0 m_e c_0^2 n_F} g(\lambda) f_{em} \tag{2}$$

where $g(\lambda)$ is the normalized line shape function expressed in the emission wavelength domain, using the equation $\int g(\lambda)\,d\lambda = 1$. The absorption cross section σ_{abs} is similar to σ_{em} via:

$$\sigma_{abs}^{X_i \to X_j}(\lambda) = \frac{e^2\lambda^2}{4\varepsilon_0 m_e c_0^2 n_F} g(\lambda) f_{abs}^{X_i \to X_j} \tag{3}$$

where $f_{abs}^{X_i \to X_j}$ is various absorption oscillator strengths $\left(X_i \longrightarrow X_j = S_0 \longrightarrow S_1,\ S_1 \longrightarrow S_n,\ T_1 \longrightarrow T_n, \text{ and } D_0^{+/-} \longrightarrow D_n^{+/-}\right)$. The normalized line shape function expressed in the emission wavelength domain, using the equation $\int g(\lambda)\,d\lambda = 1$. Considering the broadened nature, a universal Gaussian broadening with a 75 nm full-width at half-maximum (FWHM) is applied to $S_1 \longrightarrow S_0$ emission and $S_0 \longrightarrow S_1$ absorption, and a 125 nm FWHM is applied to other absorption ($X_i \longrightarrow X_j = S_1 \longrightarrow S_n$, $T_1 \longrightarrow T_n$, and $D_0^{+/-} \longrightarrow D_n^{+/-}$) for all investigated molecules. For optically pumped lasers, $S_0 \longrightarrow S_1$ self-absorption and photoinduced absorption to higher excited states $S_1 \longrightarrow S_n$ will affect the emission cross section. Therefore, the optical pumping net emission cross section $\sigma_{eff}^{net,opt}$ is defined [25]

$$\sigma_{eff}^{net,opt} = \sigma_{em} - \sigma_{abs}^{S_0 \to S_1} - \sigma_{abs}^{S_1 \to S_n} \tag{4}$$

The electrical pumping net emission cross section $\sigma_{eff}^{net,ele}$ is defined [25]

$$\sigma_{eff}^{net,ele} = \sigma_{em} - \sigma_{abs}^{S_0 \to S_1} - \sigma_{abs}^{S_1 \to S_n} - \sigma_{abs}^{T_1 \to T_n} - \sigma_{abs}^{D_0^+ \to D_n^+} - \sigma_{abs}^{D_0^- \to D_n^-} \tag{5}$$

The calculated values of descriptor A for remained 83 molecules are plotted in Fig. 4. As can be seen that six DABNA-PhCN derivative molecules, DABNA-PhCN-B, DABNA-PhCN-BFr, DABNA-PhCN-BTp, DABNA-PhCN-ID, DABNA-PhCN-MeHd and DABNA-PhCN-Tp, and two ADBNA-Me derivative molecules, ADBNA-Me-BPy and ADBNA-Me-Cx, satisfy the value range of A. DABNA-PhCN-Fr and ADBNA-Ph-BPy with the A of 0.304 and 0.303, respectively, and ADBNA-Ph-Cx with a large optical pumping emission cross section, are also included in the further screening. Among them, the electrical pump net emission cross section of eight molecules, DABNA-PhCN-BFr, DABNA-PhCN-BTp, DABNA-PhCN-MeHd, ADBNA-Me-BPy, ADBNA-Me-Cx, DABNA-PhCN-Fr, ADBNA-Ph-BPy, and ADBNA-Ph-Cx, are relatively large, making it possible to achieve electrical pump laser. The corresponding ΔE_{ST}, $\sigma_{eff}^{net,opt}$, $\sigma_{eff}^{net,ele}$ and A of 11 molecules screened above are displayed in Table 1. The values of S_1 emission cross section, various absorption cross sections at λ_{em}, and ΔE_{ST} for all molecules are displayed in Table S5–S18 in supporting information.

In order to better demonstrate the absorption situation near S_1, the stimulated emission cross section of S_1 and various above mentioned absorption cross sections (if any) in the vicinity of the emission wavelength (±125 nm, with the corresponding energy range ±0.5–1 eV) are plotted in Fig. 5. DABNA-PhCN-ID, ADBNA-Me-BPy and ADBNA-Ph-BPy suffer from a part of $S_0 \longrightarrow S_1$ self absorption, which does not seriously affect $\sigma_{eff}^{net,opt}$. Other molecules do not exhibit significant self absorption nor singlet exciton-induced losses. Except for ADBNA-Ph-Cx, other candidate molecules have almost no triplet-triplet absorption. All molecules have almost no polaron absorption. ADBNA-Ph-Cx is no longer suitable as a laser candidate due to its severe triplet exciton and polaron -induced losses. The large deviation of A between ADBNA-Ph-Cx and the minimum value 0.311×10^{-17} cm^2 eV also demonstrates the reliability of the descriptor, that is, molecules that do not meet the A range have little potential as candidate molecules for laser materials.

3.4. Photophysical properties of molecules screened by A

The main photophysical parameters for 10 remaining molecules are listed in Table 2. As can be seen that ADBNA-Ph-BPy has a very small S_1 emission rate constant and short excited state lifetime. It indicates that the molecule may not have luminescent properties, so the possibility of being a laser candidate molecule is further ruled out. ADBNA-Me-Cx is also excluded, because it also has a small k_r^S, and a larger k_{IC}^T than k_{RISC} leading to singlet harvesting less efficient. Altogether, eight molecules,

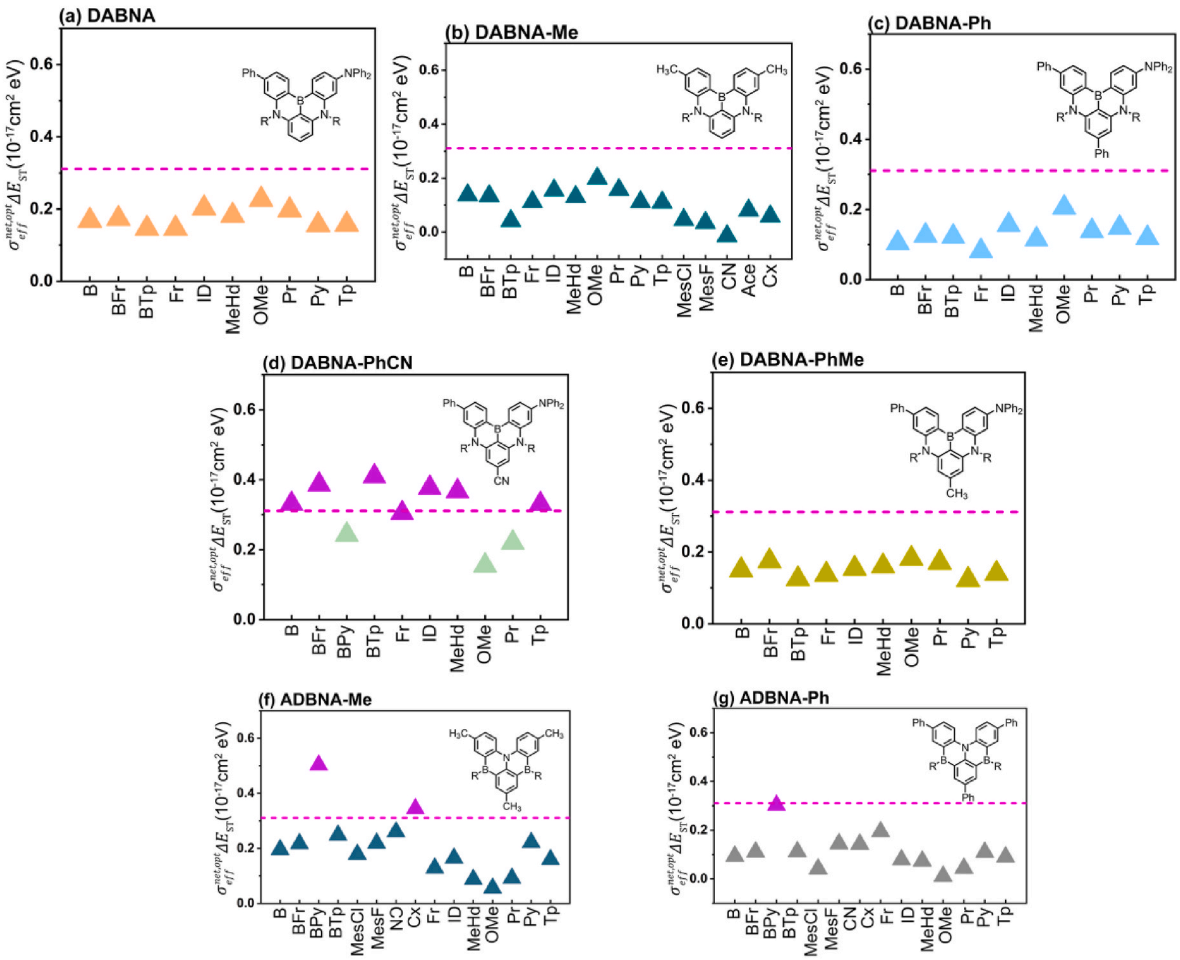

Fig. 4. The value of descriptor A for molecules with oscillator strength larger than 0.1. The A of purple triangle is larger than or close to 0.311×10^{-17} cm^2 eV.

Table 1
The energy gap between lowest singlet and triplet states (ΔE_{ST}), optical pump net emission cross section ($\sigma_{eff}^{net,opt}$), electrical pump net emission cross section ($\sigma_{eff}^{net,ele}$) and descriptor A.

molecule	ΔE_{ST} (eV)	$\sigma_{eff}^{net,opt}$ ($\times 10^{-17}$ cm^2)	$\sigma_{eff}^{net,ele}$ ($\times 10^{-17}$ cm^2)	A (cm^2 eV)
DABNA-PhCN-B	0.245	1.350	0.090	0.331
DABNA-PhCN-BFr	0.258	1.605	0.517	0.414
DABNA-PhCN-BTp	0.252	1.624	0.919	0.410
DABNA-PhCN-ID	0.268	1.406	−1.347	0.377
DABNA-PhCN-MeHd	0.240	1.528	0.298	0.367
DABNA-PhCN-Tp	0.228	1.451	0.070	0.331
ADBNA-Me-BPy	0.248	2.029	1.320	0.503
ADBNA-Me-Cx	0.189	1.825	0.386	0.344
DABNA-PhCN-Fr	0.214	1.423	0.402	0.304
ADBNA-Ph-BPy	0.142	2.126	1.466	0.303
ADBNA-Ph-Cx	0.081	2.390	0.473	0.194

including DABNA-PhCN-B, DABNA-PhCN-BFr, DABNA-PhCN-BTp, DABNA-PhCN-ID, DABNA-PhCN-MeHd, DABNA-PhCN-Tp, ADBNA-Me-BPy, and DABNA-PhCN-Fr, have relatively enormous potential as laser molecule candidate materials. In a typical four-level system, a large emission rate constant k_r^S corresponds to a small laser threshold, since k_r is directly related to the Einstein's B coefficient as expressed by the equation: $B \propto \left(\frac{c}{8\pi h\nu_0^3}\right)k_r$, which is inversely proportional to the lasing threshold. Therefore, ADBNA-Me-BPy with large k_r^S and k_{RISC} of 1.90×10^6 and 1.01×10^8 s^{-1}, respectively, may have a small laser threshold and realize electrically pumped lasing. Although the k_r^S and k_{RISC} values of DABNA-PhCN-ID are also very large, its electrical pumping net emission cross section $\sigma_{eff}^{net,ele}$ is negative, making it impossible to achieve electrically pumped laser.

Most molecules among the candidates are DABNA-PhCN derivatives. It indicates that attaching electron withdrawing substituents to rigid bodies is advantageous for lasers.

4. Conclusion

In conclusion, DFT/TDDFT for electronic structure implemented in Gaussian and TVCF formalism implemented in MOMAP package for molecular photophysical parameters are employed to investigate the potential of 119 MR-TADF molecules as laser candidate materials. A simple and effective descriptor A is proposed for quick screening the MR-TADF laser candidate molecules. A equaling to the product of ΔE_{ST} and $\sigma_{eff}^{net,opt}$, comprehensively considers both the small singlet-triplet energy gap of TADF molecules and the large emission cross section of laser molecules. Its value is greater than 0.311×10^{-17} cm^2 eV for MR-TADF laser candidate molecules. Based on our theoretical prediction, eight molecules, DABNA-PhCN-B, DABNA-PhCN-BFr, DABNA-PhCN-BTp, DABNA-PhCN-ID, DABNA-PhCN-MeHd, DABNA-PhCN-Tp, ADBNA-Me-BPy, and DABNA-PhCN-Fr, are screened as laser candidate materials through descriptor A and photophysical properties. Among them,

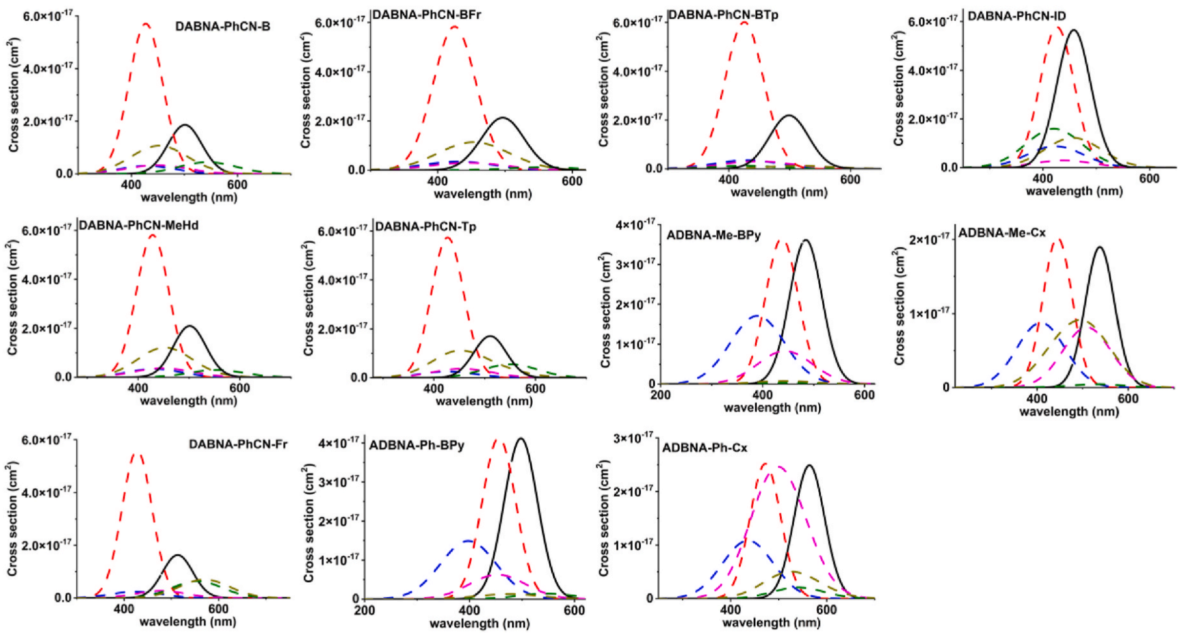

Fig. 5. Theoretically simulated S_1 emission cross sections and varied absorption cross sections. Black solid line and magenta dashed line correspond to the stimulated emission cross section and self-absorption cross section of S_1, respectively. Varied absorption cross sections introduced by $S_1 \longrightarrow S_n$ (blue dashed), $T_1 \longrightarrow T_n$ (rose madder dashed), $D_0^+ \longrightarrow D_n^+$ (blackish green dashed) and $D_0^- \longrightarrow D_n^-$ (fawn dashed) are plotted around the emission wavelength (±125 nm).

Table 2
Theoretical photophysical parameters for 11 candidates.

molecule	k_r^S (s^{-1})	k_{IC}^S (s^{-1})	k_{ISC} (s^{-1})	k_{RISC} (s^{-1})	k_{IC}^T (s^{-1})	τ_{S1} (ps)
DABNA-PhCN-B	1.55×10^5	5.40×10^9	1.77×10^5	1.19×10^5	3.03×10^4	185
DABNA-PhCN-BFr	3.56×10^4	2.06×10^9	2.41×10^4	1.97×10^4	2.20×10^2	485
DABNA-PhCN-BTp	3.29×10^4	2.03×10^9	1.29×10^4	9.85×10^3	7.88×10	492
DABNA-PhCN-ID	5.27×10^7	2.96×10^{10}	6.29×10^7	8.05×10^7	8.29×10^2	34
DABNA-PhCN-MeHd	2.00×10^5	6.52×10^9	3.11×10^5	1.97×10^5	2.28×10^2	153
DABNA-PhCN-Tp	8.96×10^4	3.68×10^9	1.01×10^5	5.27×10^4	1.60×10^4	272
ADBNA-Me-BPy	1.90×10^6	3.58×10^{10}	9.92×10^7	1.01×10^8	2.80×10^6	28
ADBNA-Me-Cx	7.57×10^3	1.38×10^9	5.64×10^4	1.45×10^4	4.38×10^6	722
DABNA-PhCN-Fr	1.19×10^5	4.42×10^9	1.63×10^5	1.03×10^5	1.29×10^4	226
ADBNA-Ph-BPy	3.04×10	1.31×10	1.11×10^2	1.34×10^2	2.41×10^5	76

ADBNA-Me-BPy with large emission rate constant of 1.90×10^6 s^{-1} and reverse intersystem crossing rate constant of 1.01×10^8 s^{-1}, corresponding to a low laser threshold, is likely to realize electrically pumped lasing. Excellent performance of laser potential of DABNA-PhCN derivatives indicates that the rigid DABNA skeleton connected with electron withdrawing substituent –CN could effectively promote the light amplification. The molecular descriptors and design strategies of MR-TADF molecules proposed in this work can provide effective guidance for the development of new laser materials.

CRediT authorship contribution statement

Rongrong Li: Writing – review & editing, Methodology, Investigation, Data curation, Conceptualization. **Zhigang Shuai:** Resources.

Declaration of competing interest

The authors declare that they have no known competing financial interests or personal relationships that could have appeared to influence the work reported in this paper.

Data availability

Data will be made available on request.

Acknowledgments

This work is supported by the National Natural Science Foundation of China (Grant No. T2350009) and the Guangdong Provincial Natural Science Foundation (Grant No. 2024A1515011185), as well as the Shenzhen city "Pengcheng Peacock" Talent Program.

Appendix A. Supplementary data

Supplementary data to this article can be found online at https://doi.org/10.1016/j.orgel.2024.107095.

References

[1] P.P. Sorokin, J.R. Lankard, Stimulated emission observed from an organic dye, chloro-aluminum phthalocyanine, IBM J. Res. Dev. 10 (1966) 162.
[2] Y. Jiang, Y.Y. Liu, X. Liu, H. Lin, K. Gao, W.Y. Lai, W. Huang, Organic solid-state lasers: a materials view and future development, Chem. Soc. Rev. 49 (2020) 5885–5944.
[3] A.S.D. Sandanayaka, T. Matsushima, F. Bencheikh, K. Yoshida, M. Inoue, T. Fujihara, K. Goushi, J.C. Ribierre, C. Adachi, Quasi-continuous-wave organic thin-film distributed feedback laser, Sci. Adv. 3 (2017) e1602570.
[4] G.Q. Wei, X.D. Wang, L.S. Liao, Recent advances in 1D organic solid-state lasers, Adv. Funct. Mater. 29 (2019) 1902981.
[5] A.J.C. Kuehne, M.C. Gather, Organic lasers: recent developments on materials, device geometries, and fabrication techniques, Chem. Rev. 116 (2016) 12823–12864.
[6] J.J. Wu, X.D. Wang, L.S. Liao, Near-infrared solid-state lasers based on small organic molecules, ACS Photonics 6 (2019) 2590–2599.
[7] H.X. Chen, M.D. Qian, K. Yu, Y.F. Liu, Low threshold microlasers based on organic conjugated polymers, FRONT CHEM 9 (2021) 807605.
[8] A.S.D. Sandanayaka, T. Matsushima, F. Bencheikh, S. Terakawa, W.J. Potscavage, C. Qin, T. Fujihara, K. Goushi, J.C. Ribierre, C. Adachi, Indication of current-

injection lasing from an organic semiconductor, Appl. Phys. Express 12 (2019) 061010.
[9] M.A. Baldo, D.F. O'Brien, M.E. Thompson, S.R. Forrest, Excitonic singlet-triplet ratio in a semiconducting organic thin film, Phys. Rev. B 60 (1999) 14422–14428.
[10] M. Lehnhardt, T. Riedl, T. Weimann, W. Kowalsky, Impact of triplet absorption and triplet-singlet annihilation on the dynamics of optically pumped organic solid-state lasers, Phys. Rev. B 81 (2010) 165206.
[11] J. Gierschner, S. Varghese, S.Y. Park, Organic single crystal lasers: a materials view, Adv. Opt. Mater. 4 (2016) 348–364.
[12] Z. Yang, Z. Mao, Z. Xie, Y. Zhang, S. Liu, J. Zhao, J. Xu, Z. Chi, M.P. Aldred, Recent advances in organic thermally activated delayed fluorescence materials, Chem. Soc. Rev. 46 (2017) 915.
[13] M. Mamada, M. Hayakawa, J. Ochi, T. Hatakeyama, Organoboron-based multiple-resonance emitters: synthesis, structure–property correlations, and prospects, Chem. Soc. Rev. 53 (2024) 1624.
[14] X. Li, Y. Wang, Z. Zhang, S. Cai, Z. An, W. Huang, Recent advances in room-temperature phosphorescence metal–organic hybrids: structures, properties, and applications, Adv. Mater. (2023) 2308290.
[15] P. Data, Y. Takeda, Recent advancements in and the future of organic emitters: TADF- and RTP-active multifunctional organic materials, Chem. Asian J. 14 (2019) 1613–1636.
[16] P. Pattanayak, A. Nandi, P. Purkayastha, Polymorphism-mediated regulation of thermally activated delayed fluorescence and room-temperature phosphorescence via intra and intermolecular charge transfer, Chem. Mater. 35 (2023) 9799–9805.
[17] P. Sivasakthi, J.M. Jacob, M.K. Ravva, P.K. Samanta, Theoretical insights into the optical and excited state properties of donor−phenyl bridge−acceptor containing through-space charge transfer molecules, J. Phys. Chem. A 127 (2023) 886–893.
[18] P.L. Santos, J.S. Ward, A.S. Batsanov, M.R. Bryce, A.P. Monkman, Optical and polarity control of donor−acceptor conformation and their charge-transfer states in thermally activated delayed fluorescence molecules, J. Phys. Chem. C 121 (2017) 16462–16469.
[19] T. Hatakeyama, K. Shiren, K. Nakajima, S. Nomura, S. Nakatsuka, K. Kinoshita, J. Ni, Y. Ono, T. Ikuta, Ultrapure blue thermally activated delayed fluorescence molecules: efficient HOMO–LUMO separation by the multiple resonance effect, Adv. Mater 28 (2016) 2777–2781.
[20] D.H. Kim, A. D'Aléo, X. Chen, A.D.S. Sandanayaka, D. Yao, L. Zhao, T. Komino, E. Zaborova, G. Canard, Y. Tsuchiya, E. Choi, J.W. Wu, F. Fages, J.L. Brédas, J. C. Ribeiro, C. Adachi, High-efficiency electroluminescence and amplified spontaneous emission from a thermally activated delayed fluorescent near-infrared emitter, Nat. Photonics 12 (2018) 98–104.
[21] Y. Cha, S. Li, Z. Feng, R. Zhu, H. Fu, Z. Yu, Organic phosphorescence lasing based on a thermally activated delayed fluorescence emitter, J. Phys. Chem. Lett. 13 (2022) 10424–10431.
[22] A. D'Aléo, M.H. Sazzad, D.H. Kim, E.Y. Choi, J.W. Wu, G. Canard, F. Fages, J. C. Ribierre, C. Adachi, Boron difluoride hemicurcuminoid as an efficient far red to near-infrared emitter: toward OLEDs and laser dyes, Chem. Commun. 53 (2017) 7003.
[23] Y. Li, K. Wang, Q. Liao, L. Fu, C. Gu, Z. Yu, H. Fu, Tunable triplet-mediated multicolor lasing from nondoped organic TADF microcrystals, Nano Lett. 21 (2021) 3287–3294.
[24] S. Li, X. Jin, Z. Yu, X. Xiao, H. Geng, Q. Liao, Y. Liao, Y. Wu, W. Hu, H. Fu, Design of thermally activated delayed fluorescent emitters for organic solid-state microlasers, J. Mater. Chem. C 9 (2021) 7400.
[25] H. Nakanotani, T. Furukawa, T. Hosokai, T. Hatakeyama, C. Adachi, Light amplification in molecules exhibiting thermally activated delayed fluorescence, Adv. Optical Mater. 5 (2017) 1700051.
[26] Q. Ou, Q. Peng, Z. Shuai, Computational screen-out strategy for electrically pumped organic laser materials, Nature Commun. 11 (11) (2020) 4485.
[27] S. Lin, Q. Ou, Z. Shuai, Computational selection of thermally activated delayed fluorescence (TADF) molecules with promising electrically pumped lasing property, ACS Materials Lett 4 (2022) 487–496.
[28] Q. Peng, Y. Yi, Z. Shuai, J. Shao, Towards quantitative prediction of molecular fluorescence quantum efficiency: role of Duschinsky rotation, J. Am. Chem. Soc. 129 (2007) 9333–9339.
[29] Z. Shuai, Q. Peng, Organic light-emitting diodes: theoretical understanding of highly efficient materials and development of computational methodology, Natl. Sci. Rev. 4 (2017) 224–239.
[30] Z. Shuai, Thermal vibration correlation function formalism for molecular excited state decay rates, Chin. J. Chem. 38 (2020) 1223–1232.
[31] M. Frisch, G. Trucks, H. Schlegel, G. Scuseria, M. Robb, J. Cheeseman, G. Scalmani, V. Barone, G. Petersson, H. Nakatsuji, et al., Gaussian 16, Gaussian. Inc., Wallingford, CT, 2016.
[32] A.D. Becke, Density-functional thermochemistry. III. The role of exact exchange, J. Chem. Phys. 98 (1993) 5648–5652.
[33] S. Grimme, Semiempirical GGA-type density functional constructed with a long-range dispersion correction, J. Comput. Chem. 27 (2006) 1787–1799.
[34] R. Krishnan, J.S. Binkley, R. Seeger, J.A. Pople, Self-consistent molecular orbital methods. XX. A basis set for correlated wave functions, J. Chem. Phys. 72 (1980) 650–654.
[35] F. Weigend, R. Ahlrichxs, Balanced basis sets of split valence, triple zeta valence and quadruple zeta valence quality for H to Rn: design and assessment of accuracy, Phys. Chem. Chem. Phys. 7 (2005) 3297–3305.
[36] F. Weigend, Accurate coulomb-fitting basis sets for H to Rn, Phys. Chem. Chem. Phys. 8 (2006) 1057–1065.
[37] A.D. Boesea, J.M.L. Martin, Development of density functionals for thermochemical kinetics, J. Chem. Phys. 121 (2004) 3405–3416.
[38] J. Tao, J.P. Perdew, V.N. Staroverov, G.E. Scuseria, Climbing the density functional ladder: nonempirical meta–generalized gradient approximation designed for molecules and solids, Phys. Rev. Lett. 91 (2003) 146401.
[39] S. Grimme, J. Antony, S. Ehrlich, H. Krieg, A consistent and accurate ab initio parametrization of density functional dispersion correction (DFT-D) for the 94 elements H-Pu, J. Chem. Phys. 132 (2010) 154104.
[40] Y. Shao, Z. Gan, E. Epifanovsky, A.T. Gilbert, M. Wormit, J. Kussmann, A.W. Lange, A. Behn, J. Deng, X. Feng, et al., Advances in molecular quantum chemistry contained in the Q-Chem 4 program package, Mol. Phys. 113 (2015) 184–215.
[41] Y. Niu, W. Li, Q. Peng, H. Geng, Y. Yi, L. Wang, G. Nan, D. Wang, Z. Shuai, Molecular Materials Property Prediction Package (MOMAP) 1.0: a software package for predicting the luminescent properties and mobility of organic functional materials, Mol. Phys. 116 (2018) 1078–1090.
[42] A. Pershin, D. Hall, V. Lemaur, J.C. Sancho-Garcia, L. Muccioli, E. Zysman-Colman, D. Beljonne, Y. Olivier, Highly emissive excitons with reduced exchange energy in thermally activated delayed fluorescent molecules, Nature Commun 10 (2019) 597.
[43] D. Hall, J.C. Sancho-García, A. Pershin, G. Ricci, D. Beljonne, E. Zysman-Colman, Y. Olivier, Modeling of multiresonant thermally activated delayed fluorescence emitters—properly accounting for electron correlation is key, J. Chem. Theory Comput. 18 (2022) 4903–4918.
[44] C.A. Guido, E. Brémond, C. Adamo, P. Cortona, Communication: one third: a new recipe for the PBE0 paradigm, J. Chem. Phys. 138 (2013) 021104.
[45] Y. Zhao, D.G. Truhlar, Design of density functionals that are broadly accurate for thermochemistry, thermochemical kinetics, and nonbonded interactions, J. Phys. Chem. A 109 (2005) 5656–5667.
[46] C. Adamo, V. Barone, Toward reliable density functional methods without adjustable parameters: the PBE0 model, J. Chem. Phys. 110 (1999) 6158–6170.
[47] S.M. Suresh, D. Hall, D. Beljonne, Y. Olivier, E. Zysman-Colman, Multiresonant thermally activated delayed fluorescence emitters based on heteroatom-doped nanographenes: recent advances and prospects for organic light-emitting diodes, Adv. Funct. Mater. 30 (2020) 1908677.
[48] A.V. Deshpande, A. Beidoun, A. Penzkofer, G. Wagenblast, Absorption and emission spectroscopic investigation of cyanovinyldiethylaniline dye vapors, Chem. Phys. 142 (1990) 123–131.